Materials and Design 30 (2009) 469–474

Contents lists available at ScienceDirect

Materials and Design

journal homepage: www.elsevier.com/locate/matdes

Microstructural characterization and mechanical properties in friction stir welding of aluminum and titanium dissimilar alloys

Y.C. Chen *, K. Nakata

Joining and Welding Research Institute, Osaka University, 11-1 Mihogaoka, Ibaraki, Osaka 567-0047, Japan

ARTICLE INFO

Article history:
Received 1 February 2008
Accepted 2 June 2008
Available online 10 June 2008

Keywords:
Welding (D)
Non-ferrous metals and alloys (A)

ABSTRACT

Al–Si alloy and pure titanium were lap joined using friction stir welding technology. Microstructure and tensile properties of joints were examined. The maximum failure load of joints reached 62% of Al–Si alloy base metal with the joints fractured at the interface. X-ray diffraction results showed that new phase of $TiAl_3$ formed at the interface. The microstructure evolution and the joining mechanism of aluminum–titanium joints were systematically discussed.

1. Introduction

The joining of titanium alloy with aluminum alloy could have a major application in the field of aerospace and automobile industry where high strength and low weight are desirable [1,2]. However, fusion welding joints between titanium and aluminum exhibit inferior mechanical properties due to the formation of brittle intermetallic phases in weld [1,3–5]. Other solid-state welding methods for joining these two materials such as pressure welding [6], diffusion bonding [7,8] and friction welding [2,9–11] processes have been reported. Wilden et al. [8] reported diffusion bonding of commercially pure Al and pure Ti. Selected mechanical testing results of joints showed that diffusion bonding was a suitable process for high strength applications. Fuji [9] studied the growth behavior of an intermediate layer in a friction-welded joint between pure Ti and pure Al. They concluded that the layer grew from the Al substrate to the Ti substrate, and neither linear time dependence nor parabolic time dependence could be used to describe the rate of layer growth. Kim et al. [10] reported the dominant factors determining the joint characteristics (strength, ductility, etc.) in friction welds between Ti and Al. They found that the joint characteristics were dominated mainly by the thickness of the intermetallic compound layer produced at the interface. The critical thickness of the intermetallic compound layer was about 5 μm. All these solid-state welding experiments showed that Ti–Al intermetallic compounds (IMC) are also found at the joint interface. In addition, diffusion bonding and friction welding have a special requirement for the geometry of welding specimens, which undoubtedly limits their application. As a novel solid-state welding technology, friction stir welding (FSW) process [12] can weld Al alloys [13–19] and Ti alloys [20–24] and get higher quality joints than fusion welding technology. These qualities are also expected when dissimilar metal materials are joined. However, researches about friction stir welding of Al and Ti have not been reported. The aim of this paper is to report the results of FSW of Ti and Al. Lap joint is selected as the joint category and the friction stir lap welding (FSLW) joint characteristics are investigated and evaluated from both mechanical and metallurgical points of view. The joining mechanism of FSLW Al and Ti is elucidated.

2. Experimental details

The base materials are a 4 mm thick ADC12 cast aluminum alloy sheet with a composition of Al-2.4–Cu-0.56–Zn-0.18–Mn-0.81–Fe-0.17–Mg-11.8–Si (mass %) and a 2 mm thick commercially available pure titanium sheet with a composition of Ti-0.045–Fe-0.057–O-0.003–N-0.002–H-0.006–C (mass %). The sheet is cut and machined into rectangular welding samples, which is 300 mm long and 100 mm wide. The samples are longitudinally lap-welded using an FSW machine. The aluminum alloy sheet is placed over the titanium sheet. The relative position of aluminum alloy and titanium in transverse direction is shown in Fig. 1. The welding parameters are at a rotation speed of 1500 rpm and at welding speeds of 60 mm/min, 90 mm/min and 120 mm/min. The upsetting force of the welding tool (made of WC–Co) used in this experiment is 5.39 kN. The shoulder diameter and probe diameter of the tool are 15 mm and 5 mm, respectively. The length of the probe is 3.9 mm and the welding tilt angle is 3°.

After welding, the joint is cross-sectioned perpendicular to the welding direction for metallographic analyses and tensile tests by an electrical-discharge cutting machine. The cross sections of the

* Corresponding author. Tel./fax: +81 6 6879 8668.
E-mail address: armstrong@hit.edu.cn (Y.C. Chen).

0261-3069/$ - see front matter © 2008 Elsevier Ltd. All rights reserved.
doi:10.1016/j.matdes.2008.06.008

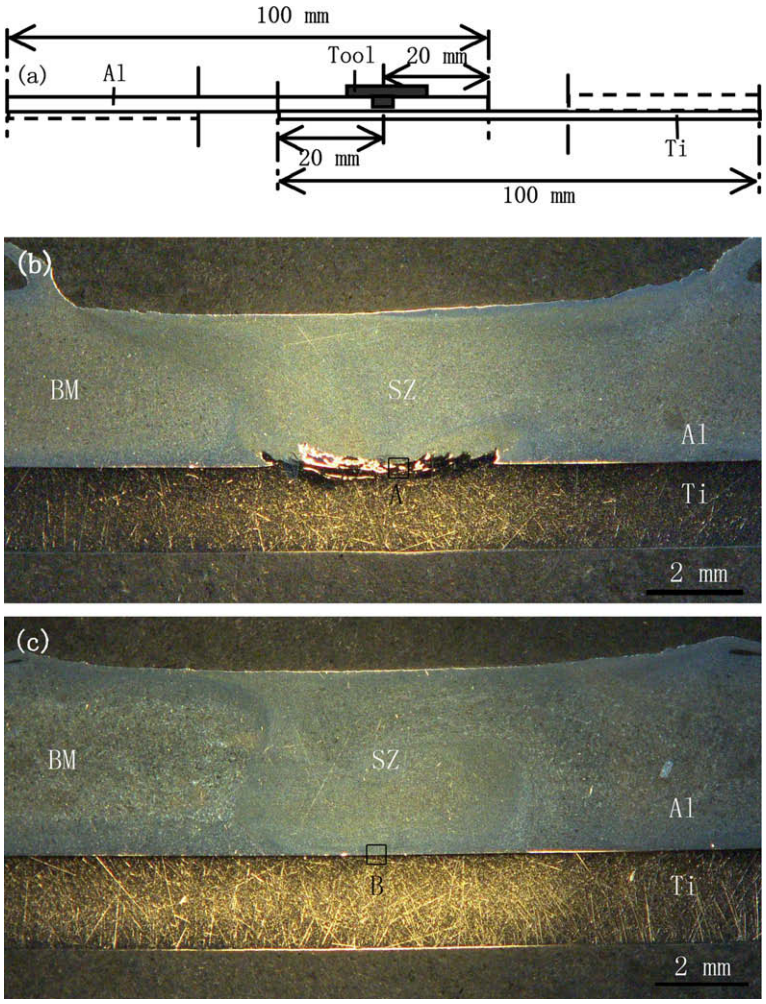

Fig. 1. Schematic diagram of a lap joint and cross-sections of joints welded at different welding speeds: (a) schematic diagram of a lap joint, (b) speed of 60 mm/min and (c) speed of 90 mm/min.

metallographic specimens are polished with a diamond polishing agent, etched with Keller's reagent (1 ml hydrochloric acid, 1.5 ml nitric acid, 2.5 ml hydrofluoric acid and 95 ml water) and are observed by a optical microscopy.

The mechanical properties of the joint are measured by the tensile tests. The tensile tests are carried out at room temperature at a crosshead speed of 1 mm/min using a tensile testing machine, and the mechanical properties of the joint are evaluated using three tensile specimens cut from the same joint. The shape of the test specimen is rectangular and the width of each specimen is 20 mm.

The interface structure and element distribution in the weld are analyzed by scanning electron microscopy (SEM) equipped with an

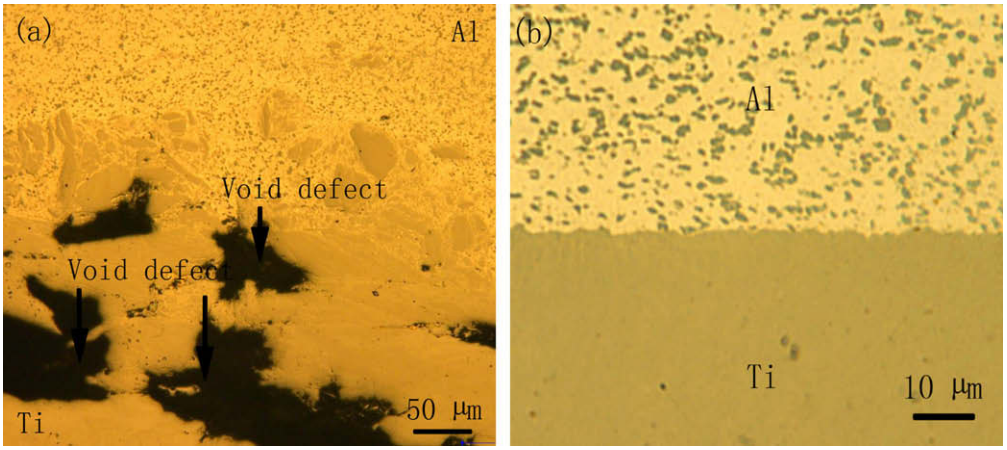

Fig. 2. Microstructural characteristic at the joining interface: (a) Region A shown in Fig. 1b and (b) region B shown in Fig. 1c.

energy dispersive X-ray spectroscopy (EDS) analysis system. Fracture surfaces of joints are analyzed using X-ray diffraction (XRD) after tensile test.

3. Results and discussion

Fig. 1 shows the schematic diagram of a lap joint and the cross-sections of joints welded at different welding speeds. At the welding speed of 60 mm/min, the tip of probe is embedded into the lower Ti sheet because of serious softening of upper Al sheet during welding. Partial Ti metal is entrapped into the stir zone (SZ) because of the stir behavior of the probe. Under the extrusion of the probe, partial Ti metal deforms and rises into the Al side along the edge of the probe (see Fig. 1b). When the welding speed increases to 90 mm/min, the tip of probe does not touch the surface of lower Ti sheet because higher welding speed effectively avoids serious softening of Al in load control mode. It can be seen from Fig. 1c that Al and Ti are joined tightly and microstructural charac-

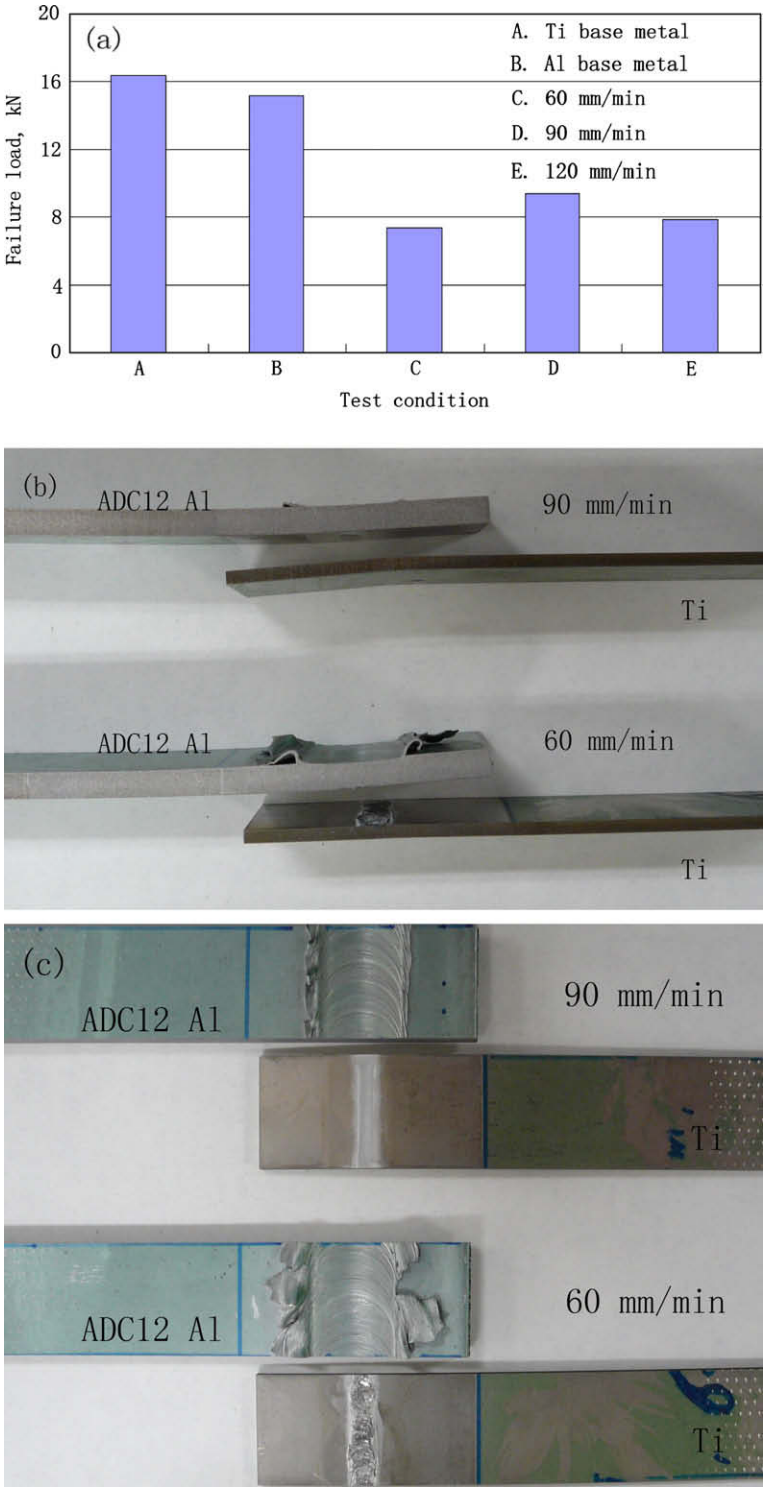

Fig. 3. Failure loads and fracture locations of joints: (a) failure load, (b) side fracture location and (c) front fracture location.

teristic in Al side is similar to that of Al alloy itself being friction stir welded. In this experiment, we are mainly concerned with the interface structure feature. Details of microstructural characteristic in the joining interface center are illustrated in Fig. 2.

Fig. 2 shows the microstructural characteristic of the joining interface of joints welded at different welding speeds. At the welding speed of 60 mm/min, the stir zone of weld contains a large amount of Ti particles (see Fig. 2a). The SZ near the interface exhibits a mixture of Al alloy and Ti particles pulled away by the forge of tool probe from the Ti side. Ti particles have an irregular shape and inhomogeneous distribution within SZ. Moreover, many void defects arise at the side of Ti because of insufficient flow behavior of Ti metal. At the welding speed of 90 mm/min, a very thin interface structure of Al and Ti instead of a mixture of Al and Ti is found. Phase structure at the interface is identified using XRD from the fracture surface after tensile test and the results will be discussed later.

The tensile test results of joints are shown in Fig. 3. The failure loads of all joints are lower than those of the base materials, and all the joints fracture at the interface. The maximum failure load, 9.39 kN, occurs at the welding speed of 90 mm/min. Failure loads of joints show lower values when the welding speeds are 60 mm/min and 120 mm/min. For the 60 mm/min joint, the decrease in failure load value is due to the welding defects in the joint, which act as cracking sources during tensile test. For the 120 mm/min joint, higher welding speed brings lower heat input and shorter reaction time of Al and Ti. Hypo-reaction undoubtedly decreases the tensile properties of joints. Fracture location results show that the joints fracture at the interface of Al and Ti and the joining region is only within the probe diameter range (see Fig. 3c). When the probe is slightly inserted into the Ti base metal, the fracture surface shows tearing feature because mixture structure of Al and Ti occurs at the interface; when the tip of probe does not touch the surface of lower Ti sheet, the fracture surface shows a flat feature.

A SEM micrograph of the interface (region A in Fig. 1b) is shown in Fig. 4. Al, Si and Ti distributions are shown in Fig. 4b, c and d, respectively. These results show that mixture structure involves Al, Si and Ti. The materials in weld zone have undergone the co-action of high temperature action and severe plastic deformation during FSW. In this case, the original coarse primary Al grains and large plate-like eutectic silicon in ADC12 base material have been transformed to fine grains and small silicon particles in the SZ. Ti in the lap interface simultaneously undergoes the synthetic effect of the thermal cycle and the mechanical cycle because of the action of friction, stir and extrusion of the probe. Thus, mixture structure forms between ADC12 SZ and Ti base metal. Al and Ti are joined by either mechanical bonding or chemical bonding or by both.

When the welding speed increases to 90 mm/min, the probe does not touch the surface of Ti. The interface structure shows a different result. A local SEM image of the interface (region B in Fig. 1c) is shown in Fig. 5. It can be seen from Fig. 5a that no significant IMC layer is produced at the interface. Al metal is pushed into the concavities of the Ti surface. EDS (line scanning analysis along the dotted line shown in Fig. 5a) analysis results vertical to the interface of joint are shown in Fig. 5b. Linear traces of Al and Ti contents show that a very thin Al–Ti layer forms at the joining interface. These results suggest that Al–Ti intermetallic compounds seem to be produced at the interface.

In order to identify the phase structure, XRD analysis of the fracture surface of joints is performed. XRD spectrums obtained from different fracture surfaces are indicated in Fig. 6. Fig. 6a shows the XRD spectrums obtained from Al sides at different welding speeds. Fig. 6b shows the XRD spectrums obtained from Ti sides. XRD result from ADC12 base metal shows that ADC12 Al alloy mainly contains Al and Si phases because ADC12 Al alloy is a hypoeutectic Al-Si alloy. XRD patterns obtained from the fracture surfaces of joints show that the phase structure in fracture surfaces

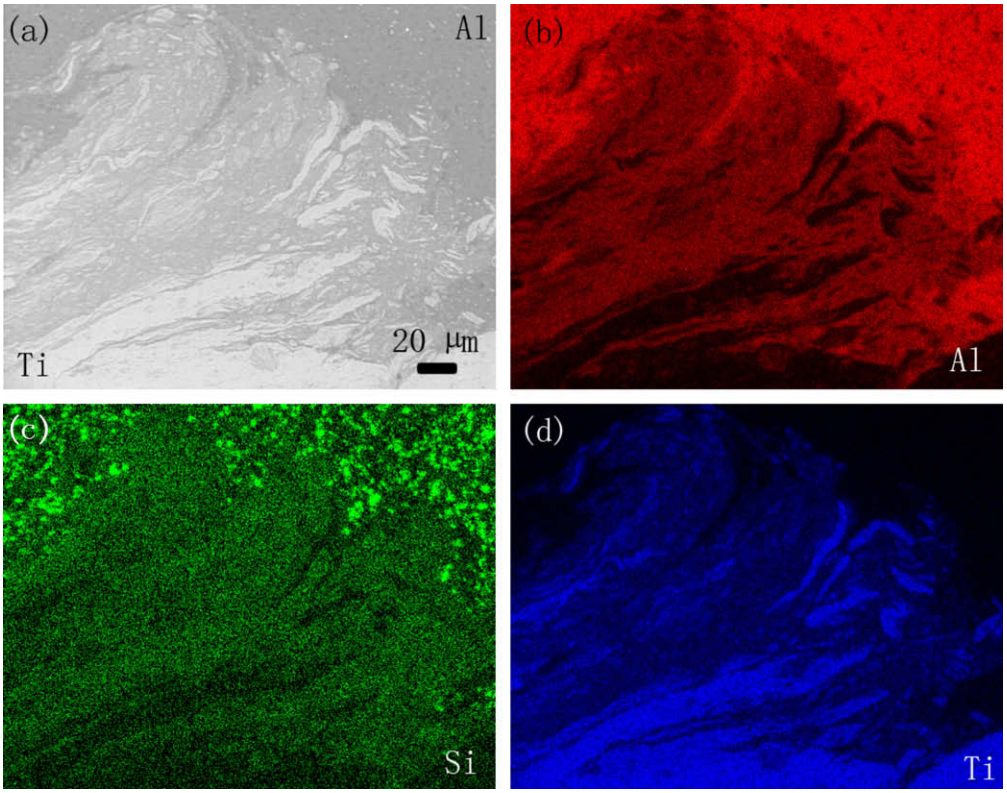

Fig. 4. Qualitative EDS map analysis of mixture structure shown in Fig. 1b, region A: (a) SEM image, (b) Al, (c) Si and (d) Ti.

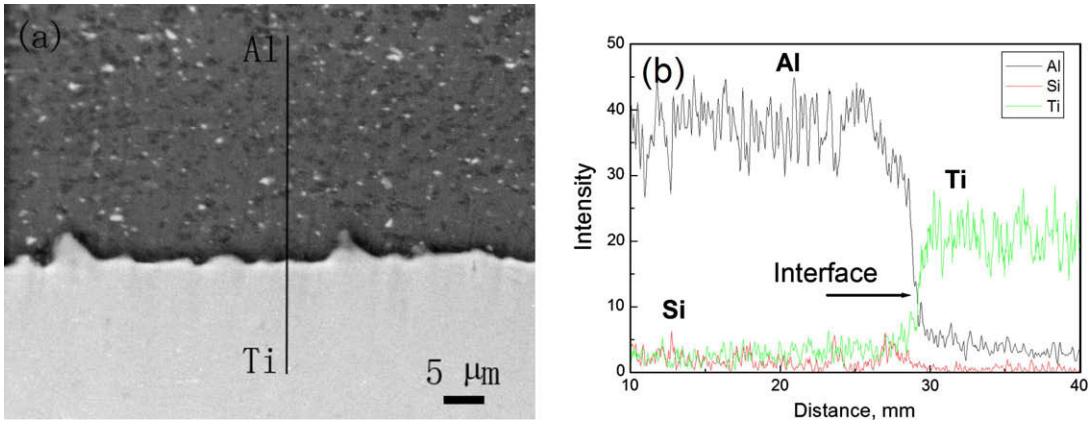

Fig. 5. Qualitative EDS line analysis of interface structure shown in Fig. 1c, region B: (a) SEM image and (b) line scanning results.

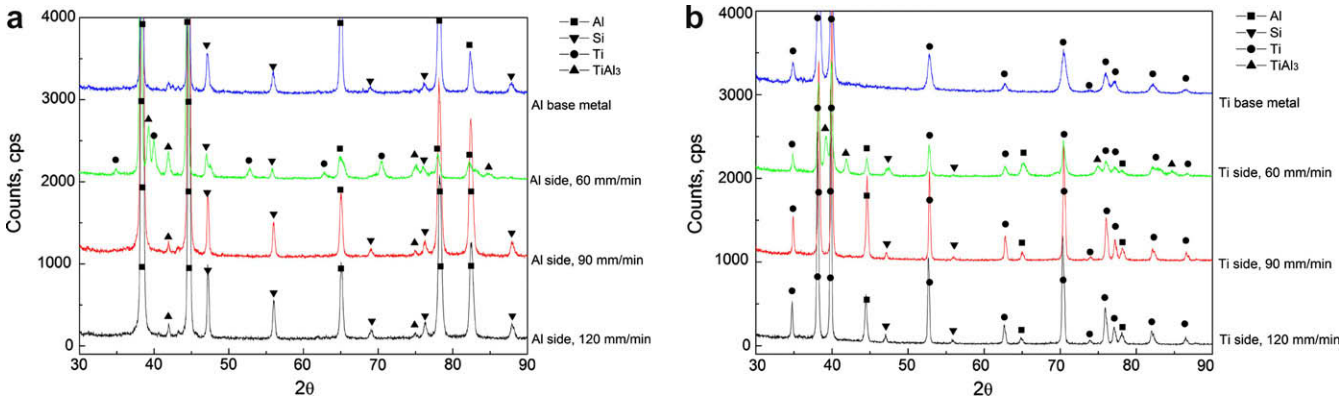

Fig. 6. XRD spectrums from different fracture surfaces: (a) from Al sides and (b) from Ti sides.

mainly contains Al, Si, Ti and $TiAl_3$ phases. Al, Si and Ti phases are from base metals that is, a new phase of $TiAl_3$ forms at the interface during welding.

Lap joints of ADC12 Al alloy and pure Ti are produced successfully using friction stir welding technology. Reaction between Al and Ti results in the formation of intermetallic phase $TiAl_3$ at the joining interface. $TiAl_3$ phase was also reported in friction welding (FW) of Al/Ti [9–11] and friction stir processing (FSP) of Al/Ti elemental powder mixtures [25]. Fuji et al. [10] reported that the dominant factor determining the joint mechanical characteristic in friction welds between Al and Ti was the thickness of the $TiAl_3$ intermetallic compound layer produced at the interface. The critical thickness of the intermetallic compound layer was about 5 μm. In our experiment, the $TiAl_3$ phase occurs in the extremely narrow region at the interface when the welding speed is 90 mm/min (see Fig. 5). The thickness of intermetallic compound layer obviously does not exceed the critical value of 5 μm. Therefore, the joint shows a considerable failure load. At the welding speed of 120 mm/min, the failure load of the joint slightly decreases because of the insufficient reaction time caused by higher welding speed. When the welding speed is 60 mm/min, excessive heat input softens the upper Al and then the tool gets inserted into the Ti base metal. Ti particles are pulled away by the forge of tool probe from the Ti side and are mixed with Al in SZ. Many large void defects arise in Ti side because of the insufficient flow behavior of Ti metal. Such defects act as cracking sources and deteriorate the tensile properties of joints during the tensile test.

The key factor of joining Al to Ti is the formation of intermetallic phases, which depends on process-related temperature–time cycles. Phase diagram of Al and Ti shows that several intermetallic compounds, namely, Ti_3Al, TiAl, $TiAl_2$, Ti_2Al_5 and $TiAl_3$ can form in this system. However, XRD results demonstrate that $TiAl_3$ phase is the only reaction product in our experiment. The formation of $TiAl_3$ as the only product had also been reported during FS Ti and Al [2,9–11]. The synthesis of titanium aluminides through powder metallurgical routes showed that $TiAl_3$ formed prior to the formation of any other titanium aluminide [26–29]. These results are consistent with thermodynamic calculations, which show that $TiAl_3$ has the lowest free energy of formation among the compounds $TiAl_3$, TiAl and Ti_3Al of Type-I aluminides. The formation of $TiAl_2$ and Ti_2Al_5 of Type-II aluminides is through a series of solid–liquid and/or solid state reactions involving TiAl as one of the starting phases [30]. Moreover, $TiAl_3$ phase is the only transient phase when the reaction temperature is lower than Al melting point [30,31]. Therefore, it is understandable that in the reaction of Ti and Al during FSW, $TiAl_3$ phase forms preferentially.

In friction stir lap joining Al and Ti, Al–Ti reaction occurs and the intermetallic phase of $TiAl_3$ forms at the interface. The sequence of joining mechanism is proposed as follows. Firstly, the metal in the lap interface undergoes the synthetic effect of the thermal cycle and the mechanical cycle because of the action of friction, stir and extrusion of the tool during FSW. Thus, high temperature and high pressure are generated at the interface. High pressure results in the rupture of surface oxide films at both sheets surface, which causes intimate contact between Ti and Al. Secondly, the heat provided by the friction stir of the tool raises the temperature high enough to initiate the exothermic reaction $Al + Ti \rightarrow TiAl_3 + Q$. The heat release further increases reaction heat,

which can enhance the reaction. Finally, $TiAl_3$ phase remains the only reaction product at joining interface because the peak temperature in Al stir zone is lower than the melting point of Al.

4. Conclusions

In summary, the following conclusions are reached. ADC12 Al alloy and pure Ti can be successfully lap welded using friction stir welding technology. The maximum failure load of lap joints can reach 62% that of ADC12 Al alloy base metal. The transient phase $TiAl_3$ forms at the joining interface by Al–Ti diffusion reaction. The formation of $TiAl_3$ is strongly dependant on welding speeds (heat inputs) during FSW and thus affects the mechanical properties of joints. A preliminary investigation of friction stir lap joining Al and Ti in the present materials indicates the feasibility of a defect-free and considerable mechanical property lap joint.

References

[1] Majumdar B, Galun R, Weisheit A, Mordike BL. Formation of a crack-free joint between Ti alloy and Al alloy by using a high-power CO_2 laser. J Mater Sci 1997;32:6191–200.
[2] Fuji A, Ameyama K, North TH. Influence of silicon in aluminium on the mechanical properties of titanium/aluminium friction joints. J Mater Sci 1995;30:5185–91.
[3] Osokin AA. Technological characteristics of the fusion welding of aluminium alloys to titanium alloys. Weld Prod 1976;23:18–20.
[4] Suoda P, Dujak J, Michalicka P. Creation of heterogeneous weld joints of titanium- and aluminium-based materials by electron beam welding. In: Welding science and technology, Japan-Slovak welding symposium, Tatranske Matliare, 1996. Department of Material Science, Institute of Scientific Instruments of the Academy of Science of the Czech Republic, p. 157–160.
[5] Michael K, Florian W, Frank V. Laser processing of aluminum–titanium-tailored blanks. Opt Lasers Eng 2005;43:1021–35.
[6] Saprygin VD. Pressure welding of aluminium–steel and titanium–aluminium transition pieces for low-temperature service. Weld Prod 1975;22:29–31.
[7] Wilden J, Bergmann JP. Manufacturing of titanium/aluminium and titanium/steel joints by means of diffusion welding. Weld Cut 2004;3:285–90.
[8] Wilden J, Bergmann JP, Herz S. Properties of diffusion welded hybrid joints titanium/aluminum. In: Brazing and Soldering: Proceedings of The 3rd International Brazing and Soldering Conference, April 24–26, 2006, Crown Plaza Riverwalk Hotel, San Antonio, Texas, USA, p. 338–43.
[9] Fuji A. In situ observation of interlayer growth during heat treatment of friction weld joint between pure titanium and pure aluminium. Sci Technol Weld Join. 2002;7:413–6.
[10] Kim YC, Fuji A. Factors dominating joint characteristics in Ti–Al friction welds. Sci Technol Weld Join. 2002;7:149–54.
[11] Fuji A, Ikeuchi K, Sato YS, Kokawa H. Interlayer growth at interfaces of Ti/Al-1%Mn, Ti/Al-46%Mg and Ti/pure Al friction weld joints by post-weld heat treatment. Sci Technol Weld Join. 2004;9:507–12.
[12] Thomas WM, Nicholas ED, Needham JC, Murch MG, Templesmith P, Dawes CJ. GB Patent Application No. 9125978.8, December 1991.
[13] Rhodes CG, Mahoney MW, Bingel WM, Spurling RA, Bampton WH. Effects of friction stir welding on microstructure of 7075 aluminum. Scripta Mater 1997;36:69–75.
[14] Mahoney MW, Rhodes CG, Flintoff JG, Spurling RA, Bampton WH. Properties of friction-stir-welded 7075 T651 aluminum. Metall Mater Trans A 1998;29A:1955–64.
[15] Sato YS, Kokawa H, Enomoto M, Jogan S. Microstructural evolution of 6063 aluminum during friction-stir welding. Metall Mater Trans A 1999;30A:2429–37.
[16] Sato YS, Kokawa H, Enomoto M, Jogan S, Hashimoto T. Precipitation sequence in friction stir weld of 6063 aluminum during aging. Metall Mater Trans A 1999;30A:3125–30.
[17] Jata KV, Semiatin SL. Continuous dynamic recrystallization during friction stir welding of high strength aluminum alloys. Scripta Mater 2000;43:743–9.
[18] Sato YS, Park SHC, Kokawa H. Microstructural factors governing hardness in friction-stir welds of solid-solution-hardened Al alloys. Metall Mater Trans A 2001;32A:3033–42.
[19] Sato YS, Kokawa H. Distribution of tensile property and microstructure in friction stir weld of 6063 aluminum. Metall Mater Trans A 2001;32A:3023–31.
[20] Pilchak AL, Juhas MC, Williams JC. Microstructural changes due to friction stir processing of investment-cast Ti–6Al–4V. Metall Mater Trans A 2007;38A:401–8.
[21] Reynolds AP, Hood E, Tang W. Texture in friction stir welds of Ti metal 21S. Scripta Mater 2005;52:491–4.
[22] Ramirez AJ, Juhas MC. Microstructural evolution in Ti–6Al–4V friction stir welds. Mater Sci Forum 2003;426–432:2999–3004.
[23] Lee WB, Lee CY, Chang WS, Yeon YM, Jung SB. Microstructural investigation of friction stir welded pure titanium. Mater Lett 2005;59:3315–8.
[24] Aonuma M, Tsumura T, Nakata K. Weldability of pure titanium and AZ31 magnesium alloy by friction stir welding. J Jpn Inst Light Met 2007;57:112–8.
[25] Hsu CJ, Chang CY, Kao PW, Ho NJ, Chang CP. Al-Al_3Ti nanocomposites produced in situ by friction stir processing. Acta Mater 2006;54:5241–9.
[26] Wang G, Dahms M. Synthesizing gamma-TiAl alloys by reactive powder processing. J Met 1993;45:52–6.
[27] Rawers JC, Wrzesinski WR. Reaction-sintered hot-pressed TiAl. J Mater Sci 1992;27:2877–86.
[28] Wang GX, Dahms M. TiAl-based alloys prepared by elemental powder metallurgy. Powder Metall Int 1992;24:219–25.
[29] Wang GX, Dahms M. Influence of heat treatment on microstructure of Ti-35 wt% Al prepared by elemental powder metallurgy. Scr Metall 1992;26:717–22.
[30] Sujata M, Bhargava S, Sangal S. On the formation of $TiAl_3$ during reaction between solid Ti and liquid Al. J Mater Sci Lett 1997;16:1175–8.
[31] Wang GX, Dahms M. Titanium aluminides from cold-extruded elemental powders with Al-contents of 25–75 at% Al. J Mater Sci 1994;29:1847–53.